On the Failure Prediction of Dual-Phase Steel and Aluminium Alloys Exposed to Combined Tension and Bending

IOP Conf. Series: Materials Science and Engineering **651** (2019) 012030 doi:10.1088/1757-899X/651/1/012030

On the Failure Prediction of Dual-Phase Steel and Aluminium Alloys Exposed to Combined Tension and Bending

Alexander Barlo[1,2*], Mats Sigvant[1,3], and Benny Endelt[2]

[1]Volvo Cars Dept. 81110 Strategy & Concept, Olofström, Sweden
[2]Department of Materials and Production, Aalborg University, Aalborg, Denmark
[3]Department of Mechanical Engineering, Blekinge Institute of Technology, Karlskrona, Sweden

E-mail: Alexander.Barlo@volvocars.com

Abstract. The interest in accurate prediction of failure of sheet metals in the automotive industry has increased significantly over the last two decades. This paper aims to evaluate two failure prediction approaches implemented in the commercial Finite Element code AutoForm^{plus} R7.04; (i) the standard Forming Limit Diagram (FLD), and (ii) the Non-linear Forming Limit Diagram. The evaluation will be testing the two approaches accuracy on predicting failure of both an AA6016 aluminium alloy and a CR440Y780T-DP dual-phase steel alloy specimen exposed to combined tension and bending. Based on the findings of this study, it is concluded that neither of the evaluated approaches is able to accurately predict failure in both cases presented.

1. Introduction

In the automotive industry today, a lot of effort is put into the failure prediction of sheet metal parts to ensure stamping process feasibility. Even though a large variety of failure prediction approaches have been proposed during the last decade, none of these have been able to replace the Forming Limit Diagram (FLD) as the industry standard within the sheet metal forming community.

At Volvo Cars Body Components, the focus on accurate failure prediction has increased over the years, and several experiments of AA6016 aluminium and CR440Y780T-DP dual-phase steel alloy specimens, exposed to combined tension and bending, have been performed. The research presented in this paper aims to evaluate two failure prediction methods implemented in the commercial Finite Element code AutoForm^{plus} R7.04:

(i) The standard Forming Limit Diagram (FLD).
(ii) The Non-linear Forming Limit Diagram.

For clarification, the term FLD is used as a description of the complete Forming Limit Diagram, containing both Forming Limit Curves (FLC) and strain fields.

The evaluation of said methods will be based on numerical models calibrated towards experiments recorded with Digital Image Correlation (DIC) to obtain the history of the forming operation.

2. Experimental Work

2.1. Experimental Setup

Experiments with punch radii of 3, 6, and 10 mm have been conducted in the setup presented in Figure 1. In the setup, the punch is moved 6 mm to the right of the model in order to eliminate the stochastic fracture location, that otherwise would be with the punch located in the centre. All tests have been run to failure, and the applied DIC is used to go back in operation history to investigate the strain development. The focus of this paper will be on the setup with a punch radius of 6 mm.

The experiments are performed as single-action draw operations with a ram velocity of 25 mm/s.

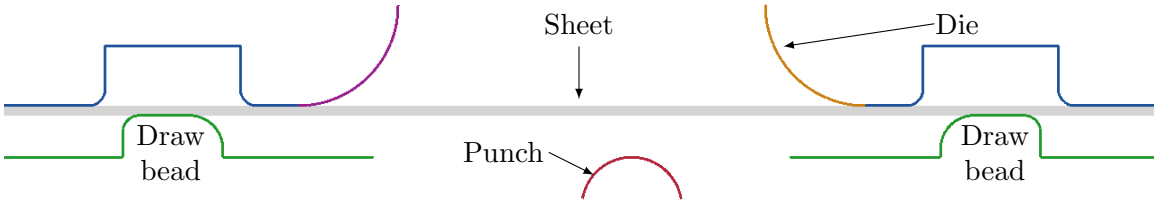

Figure 1. Cross-sectional view of the experimental setup geometry.

2.2. Experimental Repeatability

The repeatability of the AA6016 aluminium alloy is tested, to ensure the experimental data used is not an outlier.

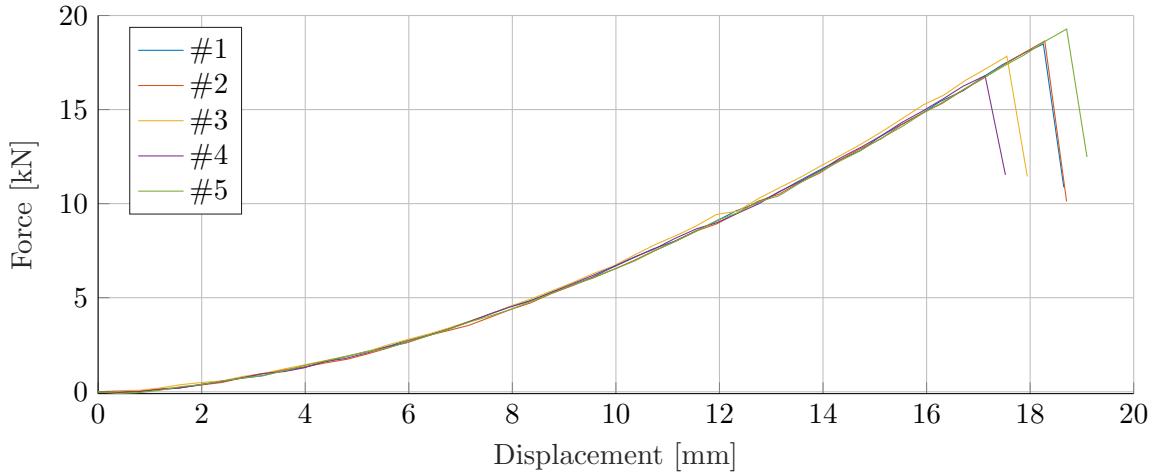

Figure 2. Force-displacement curves of the AA6016 aluminium alloy. Five tests have been conducted in order to determine repeatability.

As presented in Figure 2, the force-displacement curves of the repeated experiments align well on the force levels, but show a deviation between lowest and highest punch depth of approximately 2 mm at the point of fracture.

2.3. Neck Detection of Specimens

An undesirable phenomenon in the sheet metal forming process is failure caused by fracture. To detect if the fracture of the specimens is neck initiated, a test has been terminated approximately

0.5 mm before the fracture should occur. The punch depth of this test is based on the experiment with the lowest displacement (experiment # 4 in Figure 2). Figure 3 presents the result of this test, where a section has been examined and measured under a microscope. The outcome of the examination is that a neck in the specimen is present, why it can be concluded that the fracture is initiated by necking.

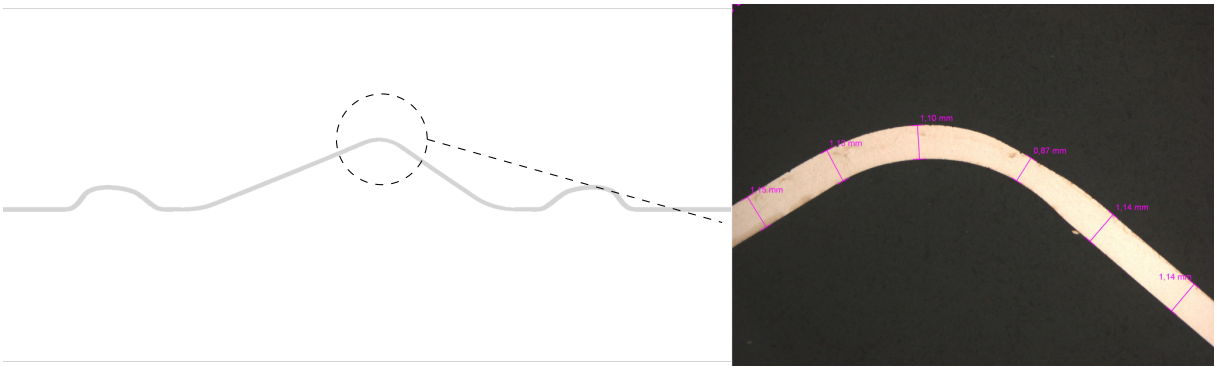

Figure 3. Cross section of an AA6016 specimen. The test has been terminated approximately 0.5 mm before fracture depth. The specimen clearly shows signs of necking.

3. Numerical Reproduction of Experiments

In order to evaluate the two failure criteria proposed, numerical reproductions of the experimental tests have been made in the commercial Finite Element code AutoForm^{plus} R7.04. Models for both the AA6016 aluminium and CR440Y780T-DP dual-phase steel alloy have been created using the elasto-plastic shell element with 11 integration points through the thickness.

3.1. Material Models

The hardening curves of the material models have been created from a combination of tensile tests and bulge tests. The applied hardening curves can be found in Figures 4 and 5.

The anisotropic behaviour is modelled using the Banabic-Balan-Comsa (BBC) yield criterion for both materials. This is done as more than 10 years of experience at Volvo Cars proves this to perform well. The same experience does however show, that the standard values for the exponent M ($M = 2 \cdot k$, 6 for BCC structure, and 8 for FCC structure [1]) need to be calibrated. The calibration of the exponent is performed by inverse modelling of the Limiting Dome Height (LDH) test.

3.2. Strain Predictions

In order to be secure accurate numerical reproductions of the experiments, a comparison of simulated and experimental major strain values is performed. The comparison is carried out by applying the DIC software ARAMIS^{TM} by GOM, where a stochastic pattern has been applied to the surface of the experimental specimens prior to testing.

Figures 6 and 7 present the major strain comparison of the numerical models and the experiments. The full lines represent the experimental data, and the dashed lines represent the numeric results. The vertical line at X = 6 mm indicates the center of the punch, and the distances in the legend describe the punch displacement distance from fracture. The predictions

Table 1. Material models used for the numerical reproduction of both the AA6016 aluminium alloy and the CR440Y780T-DP dual-phase steel alloy.

Parameter	**AA6016**	**CR440Y780T-DP**
σ_0	110.3 [MPa]	309.5 [MPa]
σ_{45}	105.9 [MPa]	307.8 [MPa]
σ_{90}	106.5 [MPa]	313.4 [MPa]
σ_b	98.3 [MPa]	307.5 [MPa]
r_0	0.732	0.678
r_{45}	0.535	0.875
r_{90}	0.677	0.848
r_b	1.01	1.02
Exponent (M)	5.7	6.2
Yield Criteria	BBC	BBC
Thickness Stress	ON	ON

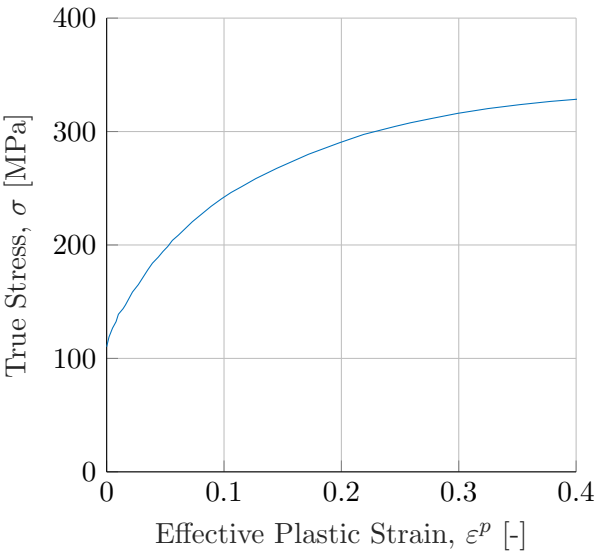

Figure 4. Hardening curve of the AA6016 aluminium alloy.

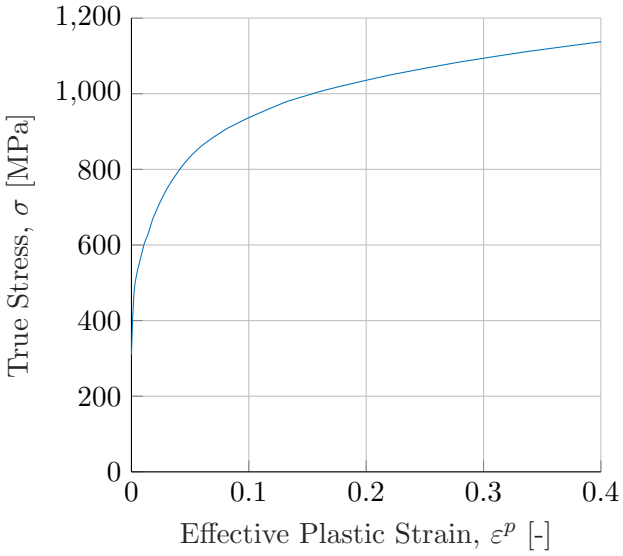

Figure 5. Hardening curve of the CR440Y780T-DP dual-phase steel alloy.

of the numerical models presented corresponds well with those of the experiments up until the last data extracted. This is believed to be due to the initialization of unstable necking, as the last data presented (red lines) are located less than 0.5 mm from fracture. The underprediction of the simulated major strain in the last stages could result in numerical models that do not indicate failure.

4. Failure Prediction

Having obtained numerical models with acceptable accuracy, the two specified failure prediction approaches can now be evaluated.

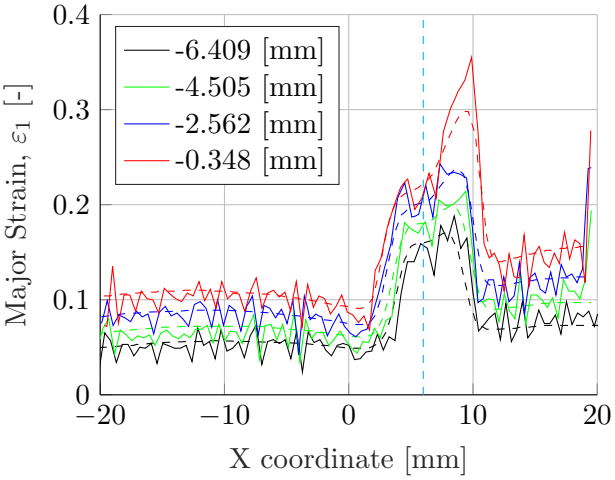

Figure 6. Major strain prediction of the AA6016 aluminium alloy numerical model. The distances presented in the legend cover both the experimental and numerical results.

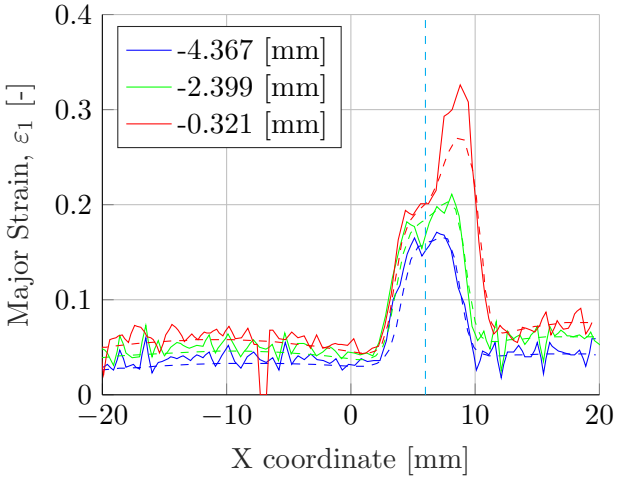

Figure 7. Major strain prediction of the CR440Y780T-DP dual-phase steel alloy numerical model. The distances presented in the legend cover both the experimental and numerical results.

4.1. Standard Forming Limit Diagram (FLD)

The Forming Limit Diagram (FLD) initially proposed by [2], has for the past many years been the industry standard within the automotive industry for predicting failure in sheet metal parts. The FLD does however require proportional loading to be applicable [3][4]. From a theoretical point of view, this would instantly reject the FLD as a suitable approach for failure prediction in specimens exposed to combined tension and bending. However, from an engineering point of view, the FLD approach is tested to investigate if the bending-under-tension load situation in the specimens could be evaluated accurately with the FLD option implemented in AutoForm^{plus} R7.04.

Figures 8 and 9 present the strain paths of the two alloys in the element with the highest major strain value at the end of the simulation. Strain paths in the bottom (blue), membrane (green), and top (black) layer are presented. As seen, the strain path in both models is far from linear in all layers included. Furthermore, indications of fracture in the top layer of both models is present, despite the numerical model underpredicting the major strain of a point in time where the specimen has not yet fractured. This leads to the conclusion that the standard FLD can not be applied to specimens exposed to combined tension and bending.

4.2. Non-linear Forming Limit Diagram

The evaluation of non-linear strain paths for failure prediction in metal sheets, is a topic that has been discussed for many years. The approach investigated in this paper, is the Non-linear Forming Limit Diagram implemented in AutoForm^{plus} R7.04 based on [5] and [6]. In short, the approach is expressed by a metamodel of a the total strain path length ratio λ, as presented in Equation 1.

$$\lambda = f(l_{pre}, \beta_{pre}, l_{post}, \beta_{post}) = \lambda_{pre} + \lambda_{post} = \frac{l_{pre}(\beta_{pre})}{l_{FLC}(\beta_{pre})} + \frac{l_{post}(\beta_{post})}{l_{FLC}(\beta_{post})} \quad (1)$$

The Non-linear Forming Limit Diagram is used to predict the onset of necking in sheets. To determine the point where an instability is introduced in the experiments, the approach proposed

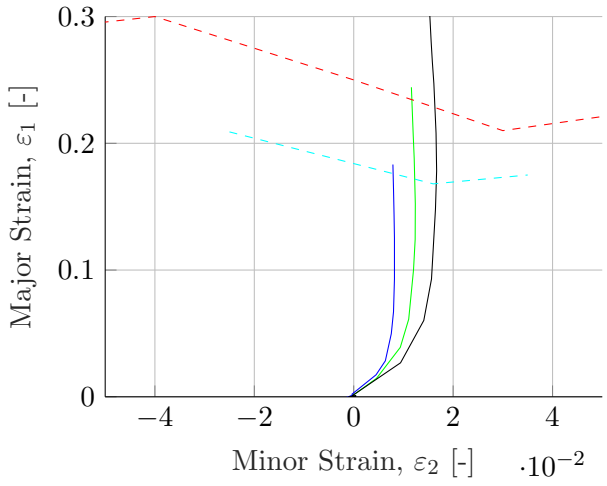

Figure 8. The strain paths of one element in the numerical model of the AA6016 aluminium alloy.

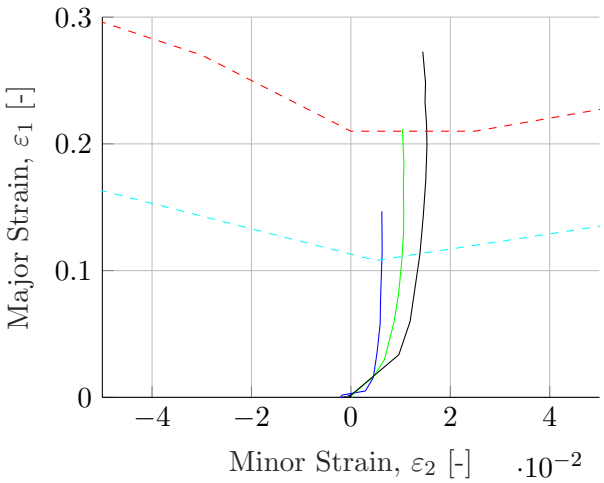

Figure 9. The strain paths of one element in the numerical model of the CR440Y780T-DP dual-phase steel alloy.

by [7], using the first derivative of the major strain with respect to time (strain rate), is applied. The instability point, determined in ARAMIS^{TM}, is then reproduced in the numerical model, and comparisons of the standard Forming Limit Diagram and the Non-linear Forming Limit Diagram can be performed. Figures 10 and 11 present the Forming Limit Diagram and the Non-linear Forming Limit Diagram of the AA6016 aluminium alloy.

The Forming Limit Diagram presented in Figure 10 reveals that the point of instability has been passed. This is in line with the findings in Section 4.1.

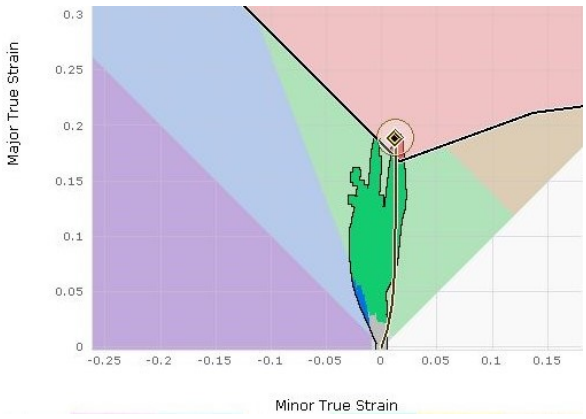

Figure 10. Forming Limit Diagram of the AA6016 aluminium alloy.

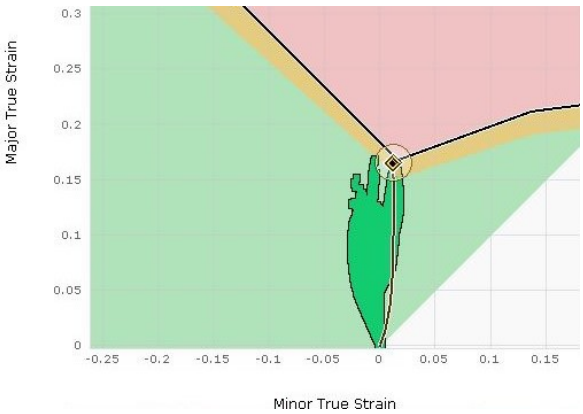

Figure 11. Non-linear Forming Limit Diagram of the AA6016 aluminium alloy.

Turning to the Non-linear Forming Limit Diagram (Figure 11), the model implemented in AutoForm^{plus} R7.04 yields a result that is acceptable, where indication of being on the border of instability is presented. This means that the Non-linear Forming Limit Diagram is an applicable approach in the case of the AA6016 aluminium alloy, but in order to accept it as a general

approach, it must also perform well for other materials and radii.

Figures 12 and 13 present the standard Forming Limit Diagram and Non-Linear Forming Limit Diagram of the CR440Y780T-DP dual-phase steel alloy. The same approach for detection of the point of instability as used in the AA6016 aluminium alloy case is applied for this case.

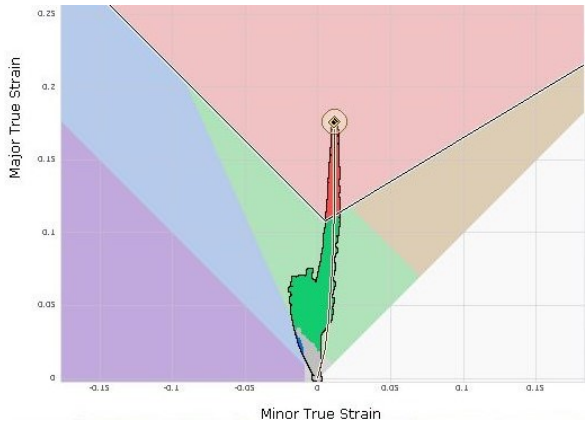

Figure 12. Forming Limit Diagram of the CR440Y780T-DP dual-phase steel alloy.

Figure 13. Non-linear Forming Limit Diagram of the CR440Y780T-DP dual-phase steel alloy.

The standard Forming Limit Diagram (Figure 12) yields that the point of instability is passed. What is interesting is that the Non-linear Forming Limit Diagram (Figure 13) also indicates that the point of instability has been passed. Furthermore, the magnitude of the strain level above the instability limit is significant and is believed not to be due to experimental uncertainties.

As the approach has not been able to predict the point of instability in both cases (both the AA6016 aluminium and CR440Y780T-DP dual-phase steel alloy), the authors of this paper can not accept the Non-linear Forming Limit Diagram as a general approach in its current implementation.

5. Conclusion

The work presented in this paper aimed to evaluate the following two failure prediction approaches implemented in the commercial Finite Element code AutoForm^{plus} R7.04 in regards to handle specimens exposed to combined tension and bending:

(i) The standard Forming Limit Diagram (FLD)
(ii) The Non-linear Forming Limit Diagram

Through comparison of experiments and numerical models, the industry standard Forming Limit Diagram proved to be not applicable due to its inability to handle the non-linear strain paths during the forming operation. The Non-linear Forming Limit Diagram yielded an accurate prediction of the AA6016 aluminium alloy, but performed poorly for the CR440Y780T-DP dual-phase steel alloy. Due to the unstable performance of the approach, the Non-linear Forming Limit Diagram is, in this paper, not accepted as a general approach.

Based on the research presented in this paper, it can be concluded that none of the evaluated approaches can be accepted as general approaches to failure prediction of specimens exposed to combined tension and bending.

6. Future Work

As presented in this paper, the two approaches evaluated were not able to accurately predict failure for all cases and failure modes. In both the stamping and crash community, a general accurate approach for predicting different failure modes is of great interest.

An interesting approach to reduce the sensitivity to non-linear strain paths in failure prediction of metal sheets, is to investigate the stress based FLD presented in e.g. [10], where the FLD in the principal strain space is transformed into the principal stress space.

Another interesting approach is the damage accumulation model GISSMO. The GISSMO model relies on tracking the damage state in different stages of the simulation in form of the plastic strain, and comparing it to a specified failure strain value dependent on both the triaxiality [8] and the Lode angle [9]. This approach will be the starting point for further research on this topic by the authors.

Yet another interesting question to raise, is where numerical models are evaluated. Both the standard Forming Limit Diagram and the Non-linear Forming Limit Diagram evaluates the models in the membrane layer, but Figures 8 and 9 present steep strain gradients across the thickness of the blank. Therefore, failure prediction approaches evaluating the blank at the top layer of the model, when exposed to combined tension and bending, is believed to be an interesting approach.

Acknowledgments

The authors of this report would like to thank Dr. Niko Manopulo from AutoForm Engineering GmbH for the interesting discussions about the Finite Element models concerning the AA6016 aluminium alloy. Furthermore, the authors would like to show their gratitude towards Prof. Dr. Wolfram Volk and Mr. Roman Norz from the Lehrstuhl für Umformtechnik und Geißereiwesen at Techniches Universität München for their assistance regarding the Non-linear Forming Limit Diagram approach.

References

[1] Banabic,D. & Sester,M.(2012), 'Influence of material models on the accuracy of the sheet metal simulations', *Material and Manufacturing Processes* **27**, 304-8.
[2] Keeler,S. & Backofen,W.(1964), 'Plastic instability and fracture in sheet stretched over rigid punches',*ASM Trans. Quart.* **56**, 25-48.
[3] Hosford,W.F. & Cadell,R.M.(2007), *Metal Forming - Mechanics and Metallurgy*, ISBN 9780521881210, 3rd edn., Cambridge University Press.
[4] Banabic,D.(2010), *Sheet Metal Forming Processes - Constitutive Modelling and Numerical Simulations*, ISBN 9783540881124, 1st edn., Springer.
[5] Volk,W. et al.(2012), 'Failure prediction for nonlinear strain paths in sheet metal forming', *CIRP Annals - Manufacturing Technology* **61**, 259-262.
[6] Volk,W. et al.(2013), 'Phenomenological and numerical description of localized necking using generalized forming limit concept', *IDDRG Proceedings 2013*, 16-21.
[7] Sigvant,M. et al.(2008), 'The definition of incipient necking and its impact on experimentally or theoretically determined forming limit curves', *Proceedings of the IDDRG2008 Conference*, Olofström, Sweden.
[8] Neukamm,F. et al.(2008), 'On closing the constitutive gap between forming and crash simulation', *10^{th} International LS-DYNA Users Conference*, 12-21.
[9] Basaran,M. et al.(2010), 'An extension of the GISSMO damage model based on lode angle dependence', *9. LS-DYNA Anwenderforum.*
[10] Stoughton, T.B. & Yoon, J.W.(2010), 'A new approach for failure criterion for sheet metals', *International Journal of Plasticity* **27**, 440-459.